Case Studies in Thermal Engineering 33 (2022) 101984

Contents lists available at ScienceDirect

Case Studies in Thermal Engineering

journal homepage: www.elsevier.com/locate/csite

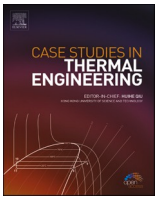

Modeling and optimization of working conditions of pyramid solar still with different nanoparticles using response surface methodology

W.M. Farouk [a], A.S. Abdullah [b,c,*], Suha A. Mohammed [d], Wissam H. Alawee [e], Z.M. Omara [f], F.A. Essa [f]

[a] Mechanical Engineering Department, Faculty of Engineering, Benha University, Egypt
[b] Mechanical Engineering Department, College of Engineering, Prince Sattam Bin Abdulaziz University, Alkharj, 16273, Saudi Arabia
[c] Mechanical Power Engineering Department, Faculty of Engineering, Tanta University, Tanta, 31734, Egypt
[d] Mechanical Engineering Department, University of Technology, Baghdad, Iraq
[e] Control and Systems Engineering Department, University of Technology, Baghdad, Iraq
[f] Mechanical Engineering Department, Faculty of Engineering, Kafrelsheikh University, Kafrelsheikh, 33516, Egypt

ARTICLE INFO

Keywords:
Pyramid solar still
Solar distillation
Response surface methodology
Cu_2O Nanoparticles
Copper oxide

ABSTRACT

The present work introduces formulating a mathematical modeling to predict the thermal performance of pyramid solar distiller (PSD) using the technique of response surface methodology (RSM) to be applied in solar distillers under different environmental parameters and nanoparticle types and concentrations. The most influential climatic process parameters considered are solar-intensity, ambient temperature, and wind velocity. The regression models for predicting the performance parameter responses were developed using RSM and a four-factor, five-level central composite architecture. The optimum parameters values obtained from RSM were predicted. The impact of various nanomaterials mixed with the water basin on PSD performance was studied. Three different nanomaterials were used (titanium oxide (TiO_2), aluminum oxide (Al_2O_3) and copper oxide (Cu_2O)). The selection of nanomaterials was considered according to their optical, thermophysical, and heat transfer properties. Effects of nanoparticles concentration on daily responses were studied. The ascertained optimal parameters were 19.5% Cu_2O concentrations, 720 w/m^2 solar-intensity, 38.6 °C ambient temperature, and 0.5 m/s wind speed for achieving the maximum productivity of PSD. Besides, the average daily productivity of Cu_2O-PSD, Al_2O_3-PSD and TiO_2-PSD at nano-concentration 0.3% was 6150, 5720 and 5300 mL/m^2.day compared to 3900 mL/m^2.day for that of conventional PSD. So, the average daily productivity increase of Cu_2O-PSD, Al_2O_3-PSD and TiO_2-PSD was 57%, 46% and 36% over PSD, respectively. Moreover, the error existed among the actual experimental and RSM coded values for P, T_w and T_g lies within 5.2%, 4.9%, and 6.5%, respectively. Evidently, this affirms the excellence of reproducibility of the pilot experimental results.

* Corresponding author. Mechanical Engineering Department, College of Engineering, Prince Sattam Bin Abdulaziz University, Alkharj, 16273, Saudi Arabia.
E-mail address: a.abdullah@psau.edu.sa (A.S. Abdullah).

https://doi.org/10.1016/j.csite.2022.101984
Received 17 January 2022; Received in revised form 19 March 2022; Accepted 27 March 2022
Available online 28 March 2022

Abbreviations

ANOVA	Analysis of Variance
PSD	Pyramid solar distiller
C	Nanoparticles' concentrations
I	Solar intensity
T_a	Ambient temperature
V_a	Wind velocity
P	Daily productivity
T_w	Water temperature
T_g	Glass temperature
CCD	Rotatable second-order design
CD	Composite desirability
D	Desirability
DF	Degree of Freedom
di	Desirability for response i
RSM	Response surface methodology
Cu_2O	Copper oxide
Al_2O_3	Aluminum oxide
b_o	Coefficient of linear term
b_i	Coefficient of Interaction term
b_{ii}	Coefficient of quadratic terms
TiO_2	Titanium oxide
H_i	Value represents the highest bound for response i
L_i	Value represents the lowest bound for response i
MS	Mean of Sequare
n	Number of responses
r_i	Signifies the desirability function weight
SS	Sum of Squares
T_i	Target value for response i
w_i	Importance weight of response i
R^2	Residuals
S/N	Signal to noise ratio

1. Introduction

1.1. Problem statement and solving motivation

Because the world greatly suffers from the shortage of fresh and potable water, desalination of brackish/saline water is the only recourse for us to confront this issue. Therefore, scientists have spent a lot of effort and time to invent different ways of desalinating salt water. For example, there are stage flashing [1], humidification-dehumidification [2,3], multi effect distillation [4], solar still [5], electrodialysis [6], and reverse osmosis [7]. Some publications reviewed the most effective modifications that were conducted on the solar stills to improve their freshwater productivity [8–12]. These reviews reported the different designs proposed by scholars such as the stepped distiller [13,14], disc distiller [15,16], vertical distiller [17,18], drum distiller [19–21], tubular distiller [22–24], trays distiller [25–27], distiller with quantum dots nanofluids [28], distiller with rotating wick belts [29,30], distiller with nanofluids [31–34], convex distiller [35,36], elevated basin distiller [37], hemispherical distiller [38], pyramid distiller [39,40], distiller with finned absorbers [41–43], distiller with corrugated absorbers [44–46], distiller with phase change materials [47], and distiller with condenser [48,49].

1.2. Pyramid solar distiller (PSD) recent background

PSD has a square projected area with a pyramid-shaped glass cover consisted of four triangles glass sheets welded together to from the pyramid shape. Various studies were performed to enhance PSD performance. Al-Madhhachi and Smaisim [50] tested experimentally and numerically the performance of PSD through the four seasons of the year. Also, they elaborated the difference between the triangle, pyramid, and pentagon distillers. Results revealed that the pentagon distiller obtained higher productivity and efficiency than the others. Prakash and Jayaprakash [51] created four steps inside PSD to increase its inside absorbing area. They reached a thermal efficiency of 50.85% with a productivity of 3.25 L/day. Also, Alawee et al. [52] proposed a different design of PSD. They installed four rotating cylinders and three electric heaters inside the PSD to increase the evaporative and exposure surface areas. They augmented the productivity by 214%, where the productivities of the modified and conventional PSDs were 9.1 and 2.9 L/m^2.day, respectively. Moreover, Essa et al. [53] tested experimentally and theoretically the performance of PSD with focusing reflectors,

Fig. 1. Photograph of the experimental setup.

continuous cooling cycle, and dangled cords of wicks on the distiller absorber. Results obtained that the productivity of the modified PSD was improved by 195% as compared to that of the conventional PSD. Besides, Modi and Nayi [54] examined the influence of using forced evaporation, granite as a heat storing material, and forced condensation on the output productivity of PSD at various water depths (2 and 3 cm). The distillate of PSD with the mentioned modifications was augmented by 61.53%. Moreover, Alawee et al. [55] created a parallel surface to the main absorber of PSD and dangled wick ropes from the upper surface to the lower one. The number of wick ropes was investigated. They found that the performance of PSD was best at 25 wick ropes, where the productivity of PSD was augmented by 122% and thermal efficiency was 53%. Additionally, Elgendi et al. [56] compensated the distilled water of PSD using automatic feed water mechanism in an attempt to optimize the performance of PSD. Besides, Kabeel and Abdelgaied [57] increased the performance of PSD via cooling the glass cover and installing graphite surface inside the distiller to work as sensible storing medium. Therefore, they augmented the PSD productivity by 6.5%. Shanmugapriya et al. [58] tested thermophysically the performance of acrylic PSD with and without Zn^{2+} substituted Cr_2O_3 nanomaterials. They reported a productivity of 3.628 L/day for the modified distiller.

1.3. Response surface methodology (RSM)

RSM is a method that combines mathematical laws and statistics to analyze problems in which many independent variables affect the response. The main objective of RSM is to get the best values for the variables that give the optimal response performance. This method also gives a regression model that relates the variables to process response. In addition, this productive relationship can be used to predict the system response when process parameters vary within predetermined ranges. The obtained regression model symbolizes geometrically the surface, when plotted as a response against any two process parameters. These plots illustrate visually the relationship between response and process parameters. Then, from these contour figures, the optimal values for the parameters affecting the system performance can be visually reported.

The RSM method has been used in many applications, and it has proven its effectiveness as a numerical method by comparing it with experimental studies and other numerical studies. Ziehyun et al. [59] used a response surface methodology and artificial neural network to build a model of a NOx removal system in a LNG terminal that estimates the released amounts of NOx in flue gas from a submerged combustion vaporizer. A response surface methodology was applied by Filipa Paulo and Lúcia Santos [60] to obtain eugenol-loaded ethyl cellulose microparticles. El-Taweel and Gouda [61] used response surface methodology discusses the feasibility of using a wire as a tool in electrochemical turning process (WECT). This study measures the performance criteria of the WECT process through investigating the effect of working parameters, namely, wire diameter, wire feed rate, work piece rotational speed, applied voltage, and overlap distance, on metal removal rate and, surface roughness.

1.4. Aim of study

Depending on the above literature, we did not find, to the authors knowledge, a mathematical model describing the productivity of PSD under different climatic conditions. Then, this study was carried out using a new method RSM, and the effect of nanoparticles was also studied. So, the novelty of this present work can be pointed. This work introduces a different formulation of a mathematical modeling using a novel technique to be applied in the solar distillers with environmental parameters and concentration of nanoparticles to predict the responses of freshwater productivity and temperatures of water and glass of PSD. In addition, what distinguishes this method is that the built models for the performance evaluating parameters could be applied in any case of solar distillers with and without nanomaterials. The parameters of solar intensity, ambient temperature, and wind velocity were considered as the most effective environmental factors. The regression models for predicting the responses of performance parameters are developed using RSM and a four-factor with five-level central composite architecture. Moreover, the impact of various nanomaterials mixed with the water basin on PSD performance was studied. Three different nanomaterials were investigated (TiO_2, Al_2O_3, and Cu_2O). Additionally, the effects of nanoparticles' concentrations on daily responses of PSD were studied. The optimum values of varying parameters obtained from RSM were also predicted.

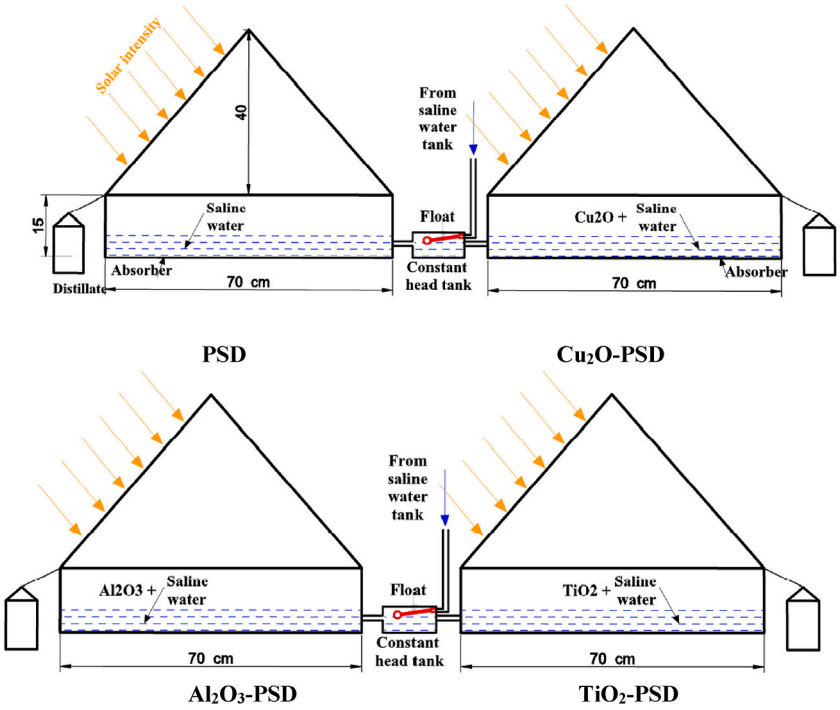

Fig. 2. Schematic of the investigated distillers.

Table 1
Properties of nanomaterials used.

Chemical composition	Size (nm)	Density (g/cm^3)	Thermal conductivity (W/m·K)	Specific heat (J/kg.K)
Cu_2O	10–20	~6.31	~76.5	~540
Al_2O_3	10–20	~3.95	~40	~525
TiO_2	10–20	~4.05	~11.8	~695

2. Experimental elaboration

2.1. Setup fabrication

The whole setup is shown in Fig. 1 and Fig. 2. The setup combined four similar pyramid solar stills: conventional pyramid solar distiller (PSD), pyramid solar distiller with copper oxide nanoparticles (Cu_2O-PSD), pyramid solar distiller with aluminum oxide nanoparticles (Al_2O_3-PSD), and pyramid solar distiller with titanium oxide nanoparticles (TiO_2-PSD). Other components of the setup were the feed water reservoir and two constant head water tanks as shown in Fig. 2. The feed water reservoir was dimensioned as 50 cm (length) × 50 cm (width) × 100 cm (height). In addition, each constant head tank was installed to control the basin water depth of two distillers. The constant head tank was a cylindrical plastic tank with a diameter of 25 cm and a length of 35 cm. It was connected to the main water reservoir and distillers. The height of the water was controlled by a float inside the constant head tank. Also, the required measuring devices were connected to the system. The properties of Cu_2O, Al_2O_3, and TiO_2 are obtained in Table 1.

All solar distillers were made of 1.5 mm thick galvanized steel. Also, the solar stills had a square base of 70 cm × 70 cm (identical areas) as shown in Fig. 2. Besides, all solar stills had vertical walls of 15 cm, Fig. 2. These dimensions were chosen to have a base area of 0.5 m^2. The base of distiller was made of galvanized iron and it was painted black to increase the absorption of solar radiation. In addition, a cover of four glass triangles (with four edges) was fixed on the four walls of the distiller base, Fig. 1. Also, the glass cover was 4 mm thick. Every glass triangle was an equilateral triangle with a base length of 70 cm. The height of the triangle was 53 cm, and the side length was 63.5 cm. The four glass triangles were installed at an inclination angle of 49° with horizontal. A circular trough was fixed on the inner surface of the four glass triangles at their lower ends. The function of this circular trough was to accumulate the droplets condensed on the inner glass walls. After that, the accumulated distillate was collected into external flasks through a hose, and the productivity quantity was determined by a sensitive balance. Additionally, a fiberglass (5 cm thick) was used as an insulation for the basin distiller to eliminate the heat loss to the ambient. Also, a thermal silicone was used as a sealing material for all contact edges either for the glass edges or steel edges.

Table 2
Properties of the measuring devices.

Device	Dimension	Unit	Resolution	Accuracy	Range	Error
Solarimeter	Solar irradiance	W/m^2	0.1	±1	0–5000	1.6%
K-type thermocouple	Temperature	°C	0.1	±0.5	0–100	1.3%
Anemometer	Air speed	m/s	0.01	±0.1	0.4–30	1.1%
Balance	Distillate	kg	0.01	±0.2	0–25	1.3%

Table 3
Coded and actual values of input variables.

Input parameters	Symbol	Levels					Outputs
		−2	−1	0	+1	+2	
Concentration of nano Cu_2O (C), %	X_1	0	0.1	0.2	0.3	0.4	(P), (T_w), (T_g)
Solar intensity (I), W/m^2	X_2	600	630	660	690	720	
Ambient temperature (Ta), °C	X_3	36	37	38	39	40	
Wind velocity (Va), m/s	X_4	0.5	1	1.5	2	2.5	

2.2. Measuring instruments

As well known, the solar still performance is evaluated based on the parameters of solar radiation, temperatures, amount of distillate, and ambient air speed. Experimentally, these parameters were measured with the help of appropriate devices. So, a solar pyranometer was used to know the value of solar radiation at different times of the day. Also, the temperature was measured using K-type thermocouples. Besides, an anemometer was used to measure the ambient air speed. Finally, the productivity was measured by a sensible balance. The readings were recorded every hour through the daytime. Table 2 tabulates the properties of the measuring instruments.

2.3. Experimental planning

As well known, RSM is a consecutive procedure. In the current research, the nanoparticles' concentrations of Cu_2O (C), solar intensity (I), ambient temperature (T_a), and wind velocity (V_a) circumstances were chosen after conducting the pilot experimentations. Both actual and coded values of RSM variables were presented in Table 3. Experimentations were performed based on the proposed procedures regarding the central composite rotatable second-order design (CCD). Corner-16, axial-8, and center-6 are a total of 30 points in CCD with 2β fractional factorial points [62]. The matrix of experimental design, outcomes, and composite desirability that obtains the coded and actual parameters data is tabulated in Table 4. ANOVA analysis is adopted to investigate the significance of the working conditions on the characteristics of PSD and to detect which condition has the most predominant impact. The following steps were adopted for the DOE:

1 Primary runs were executed to find the effective rang of process conditions as indicated in Table 3.
2 RSM was applied to design the experimental work.
3 The working conditions of RSM were performed experimentally.
4 The statistical analysis was implemented for discovering the relation amongst the input factors and output response for PSD with three different nanomaterials (Cu_2O, Al_2O_3, and TiO_2).
5 Discussion of the statistical analysis results,
6 Developing the optimization model of the process.
7 Discussion of the optimization model's results.

3. Modeling and adequacy regarding the RSM

The intended response modeling to numerous independent input factors can be achieved utilizing the experiments design and regression analyses. The following is a representation of RSM:

$$Y_u = f(X_1, X_2, X_3, \ldots . X_k) \pm \varepsilon \tag{1}$$

where Y_u, X, and ε are the corresponding response function, input variables of coded quantities, and fitting error of the uth observances, respectively. As a result, when considering the investigated parameters of $C,\ I,\ T_a$ *and* V_a (as stated in section 2.3), a quadratic model is suggested. The quadratic modeling of Y_u is [62]:

$$Y_u = b_o + \sum_{i=1}^{k} b_i X_i + \sum_{j>i}^{k} b_{ij} X_i X_j + \sum_{i=1}^{k} b_{ii} X_i^2 \pm \varepsilon \tag{2}$$

where the coefficients b_o, b_i, b_{ij} and b_{ii} are the free, linear, interaction, and quadratic terms, respectively. Then, using the values tabulated in Table 4, the full models framework can be obtained.

ANOVA variance analysis tool was utilized to check the models' adequacies. First, we calculated the value of the developed models

Table 4
Design of experiments, outcomes, and composite desirability of Cu_2O-PSD process.

No. of exp.	Concentration of nano Cu_2O (C), % (X_1)		Solar intensity (I), W/m^2 (X_2)		Ambient temperature (Ta), °C (X_3)		Wind speed (Va), m/s (X_4)		Daily Productivity, (P)	Water temperature, (T_w)	Glass temperature, (Tg)	Composite desirability
	Coded	Actual	Coded	Actual	Coded	Actual	Coded	Actual				
1	−1	0.10	−1	630	−1	37	−1	1	4500	60.8	42	0.202569
2	1	0.30	−1	630	−1	37	−1	1	5480	60.5	43	0.192544
3	−1	0.10	1	690	−1	37	−1	1	5200	61.3	42	0.259901
4	1	0.30	1	690	−1	37	−1	1	6400	61.4	44	0.459678
5	−1	0.10	−1	630	1	39	−1	1	4700	63	41	0.550752
6	1	0.30	−1	630	1	39	−1	1	5800	61.7	45	0.451015
7	−1	0.10	1	690	1	39	−1	1	5400	64.1	38	0.826508
8	1	0.30	1	690	1	39	−1	1	6450	63.4	43	0.956588
9	−1	0.10	−1	630	−1	37	1	2	4950	60.4	42	0.273008
10	1	0.30	−1	630	−1	37	1	2	5850	61.3	38	0.600012
11	−1	0.10	1	690	−1	37	1	2	5400	60.7	46	0.0082822
12	1	0.30	1	690	−1	37	1	2	6300	62	42	0.288107
13	−1	0.10	−1	630	1	39	1	2	5050	62.4	44	0.384586
14	1	0.30	−1	630	1	39	1	2	5950	62.4	43	0.563905
15	−1	0.10	1	690	1	39	1	2	5600	63.5	45	0.305532
16	1	0.30	1	690	1	39	1	2	6400	63.7	45	0.565802
17	−2	0	0	660	0	38	0	1.5	4000	62	41	0
18	2	0.4	0	660	0	38	0	1.5	6050	62	42	0.450361
19	0	0.2	−2	600	0	38	0	1.5	5300	61.5	41.5	0.605623
20	0	0.2	2	720	0	38	0	1.5	6500	63	43.3	0.732985
21	0	0.2	0	660	−2	36	0	1.5	5750	60	42.5	0
22	0	0.2	0	660	2	40	0	1.5	6100	64	43.5	0.619006
23	0	0.2	0	660	0	38	−2	0.5	5700	62	43.1	0.554116
24	0	0.2	0	660	0	38	2	2.5	6200	62	45	0.350068
25	0	0.2	0	660	0	38	0	1.5	5900	62	43	0.526326
26	0	0.2	0	660	0	38	0	1.5	5900	62	42	0.518326
27	0	0.2	0	660	0	38	0	1.5	5900	62	43	0.536326
28	0	0.2	0	660	0	38	0	1.5	5900	62	43	0.546326
29	0	0.2	0	660	0	38	0	1.5	5900	62	43	0.526326
30	0	0.2	0	660	0	378	0	1.5	5900	62	43	0.526326

Table 5
ANOVA for quadratic model - Response 1 - daily productivity (P).

Source	SS	*df*	MS	F value	*P* value	*Contribution %*
M	1.010E+07	14	7.213E+05	106.55	<0.0001(significant)	6.67
X_1	5.831E+06	1	5.831E+06	861.40	<0.0001	50.1
X_2	2.202E+06	1	2.202E+06	325.32	<0.0001	24.35
X_3	1.617E+05	1	1.617E+05	23.89	0.0002	1.5
X_4	2.752E+05	1	2.752E+05	40.65	<0.0001	2.54
X_1^2	1.476E+06	1	1.476E+06	218.05	<0.0001	13.64
X_2^2	10407.44	1	10407.44	1.54	0.2341	0.096
X_3^2	4800.30	1	4800.30	0.7091	0.4130	0.044
X_4^2	1336.01	1	1336.01	0.1974	0.6632	0.0123
X_1X_2	306.25	1	306.25	0.0452	0.8344	0.0028
X_1X_3	1056.25	1	1056.25	0.1560	0.6984	0.0098
X_1X_4	43056.25	1	43056.25	6.36	0.0235	0.0397
X_2X_3	1806.25	1	1806.25	0.2668	0.6130	0.0167
X_2X_4	71556.25	1	71556.25	10.57	0.0054	0.661
X_3X_4	4556.25	1	4556.25	0.6731	0.4248	0.0421
Residual	1.015E+05	15	6769.44			0.063
Lack of Fit	1.015E+05	10	10154.17			0.094
Pure Error	0.0000	5	0.0000			0
Cor Total	1.020E+07	29				

Table 6
ANOVA for quadratic model - Response 2 - water temperature (T_w).

Source	SS	*df*	MS	F value	*P* value	*Contribution %*
M	31.33	14	2.24	411.01	<0.0001(significant)	6.68
X_1	0.0017	1	0.0017	0.3061	0.5882	0.005
X_2	4.68	1	4.68	859.90	<0.0001	18.94
X_3	23.60	1	23.60	4335.00	<0.0001	65.33
X_4	0.0017	1	0.0017	0.3061	0.5882	0.005
X_1^2	0.0005	1	0.0005	0.0875	0.7715	0.0015
X_2^2	0.0933	1	0.0933	17.14	0.0009	0.28
X_3^2	0.0005	1	0.0005	0.0875	0.7715	0.0015
X_4^2	0.0005	1	0.0005	0.0875	0.7715	0.0015
X_1X_2	0.1600	1	0.1600	29.39	<0.0001	0.476
X_1X_3	0.9025	1	0.9025	165.77	<0.0001	2.68
X_1X_4	1.32	1	1.32	242.91	<0.0001	3.93
X_2X_3	0.4900	1	0.4900	90.00	<0.0001	1.46
X_2X_4	0.0400	1	0.0400	7.35	0.0161	0.12
X_3X_4	0.0225	1	0.0225	4.13	0.0602	0.07
Residual	0.0817	15	0.0054			0.016
Lack of Fit	0.0817	10	0.0082			0.0244
Pure Error	0.0000	5	0.0000			0
Cor Total	31.41	29				

(F) then, we compared its values with the standard F values for the desired confidence levels (99.34%, 96.9% and 96.9% for P, T_w and T_g, respectively). The built models would be in confidence level if their F values do not pass the standard F values [63]. ANOVA tables for daily productivity (P), water temperature (T_w), and glass temperature (T_g) of PSD for Cu_2O nanomaterial are presented in Table 5, Table 6, and Table 7, respectively.

From the above analysis and after eliminating the non-significant terms, the final response equations for P, T_w and T_g are:

1 **Mathematical model for daily productivity (P) with Cu_2O nanoparticles**

$$P = -50668.23 + 17889.58\,C + 58.52\,I + 1388.13Ta + 4730.42\,Va + 1.46\,C \times I - 81.25C * Ta - 1037.5\,C \times Va - 0.35\,I \times Ta - 4.46\,I \times Va - 33.75\,Ta \times Va - 23197.9\,C^2 - 0.022\,I^2 - 13.23\,Ta^2 - 27.9\,Va^2 \quad (3)$$

2 **Mathematical model for water temperature (T_w) with Cu_2O nanoparticles**

$$Tw = +163.52 + 59.86\ C - 0.29\ I - 1.95\ Ta + 3.97\ Va + 0.033\ C \times I - 2.38\ C \times Ta + 5.75\ C \times Va + 0.006\ I \times Ta - 0.0033\ I \times Va - 0.075\ Ta \times Va - 0.42\ C^2 + 0.00007\ I^2 - 0.004\ Ta^2 - 0.017Va^2 \quad (4)$$

Table 7
ANOVA for quadratic model - Response 3 - glass temperature (T_g).

Source	SS	*df*	MS	F value	*P* value	*Contribution %*
M	90.45	14	6.46	80.15	<0.0001(significant)	6.712
X_1	1.04	1	1.04	12.92	0.0027	1.081
X_2	4.68	1	4.68	58.08	<0.0001	4.86
X_3	2.04	1	2.04	25.33	0.0001	2.12
X_4	4.86	1	4.86	60.29	<0.0001	5.05
X_1^2	3.20	1	3.20	39.72	<0.0001	3.33
X_2^2	0.3733	1	0.3733	4.63	0.0481	0.39
X_3^2	0.0305	1	0.0305	0.3781	0.5479	0.032
X_4^2	2.40	1	2.40	29.78	<0.0001	2.49
X_1X_2	0.5625	1	0.5625	6.98	0.0185	0.584
X_1X_3	10.56	1	10.56	131.03	<0.0001	10.97
X_1X_4	27.56	1	27.56	341.92	<0.0001	28.64
X_2X_3	7.56	1	7.56	93.81	<0.0001	7.86
X_2X_4	14.06	1	14.06	174.45	<0.0001	14.61
X_3X_4	10.56	1	10.56	131.03	<0.0001	10.97
Residual	1.21	15	0.0806			0.086
Lack of Fit	0.3758	10	0.0376	0.2255	0.9783 (not significant)	0.039
Pure Error	0.8333	5	0.1667			0.173
Cor Total	91.66	29				

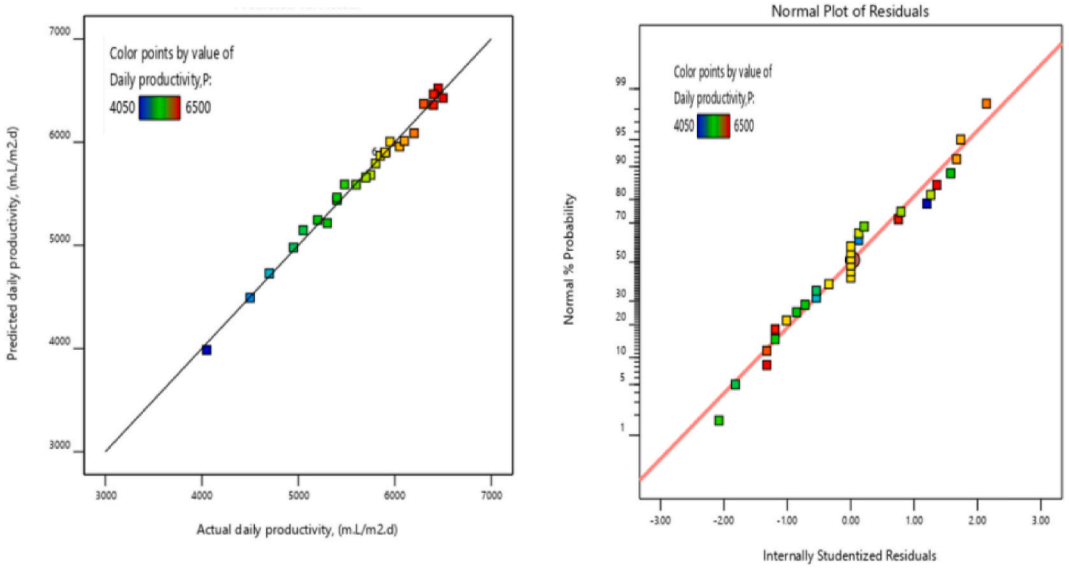

(a) Experimental versus predicted values (b) Normal residuals plot

Fig. 3. Experimental versus predicted values and Normal residuals plot for daily productivity (*P*).

3 Mathematical model for glass temperature (T_g) with Cu_2O nanoparticles

$$\mathrm{Tg} = -344.9 - 294.88\ \mathrm{C} + 0.95\ \mathrm{I} + 8.8\ \mathrm{Ta} - 100.4\ \mathrm{Va} + 0.06\ \mathrm{C}\times\mathrm{I} + 8.13\ \mathrm{C}\times\mathrm{Ta} - 26.25\ \mathrm{C}\times\mathrm{Va} - 0.023\ \mathrm{I}\times\mathrm{Ta} + 0.063\ \mathrm{I}\times\mathrm{Va} + 1.630\ \mathrm{Ta}\times\mathrm{Va} - 34.17\ \mathrm{C}^2 - 0.0001\ \mathrm{I}^2 + 0.033\ \mathrm{Ta}^2 + 1.18\ \mathrm{Va}^2 \quad (5)$$

Through these equations and by knowing the percentage of Cu_2O nanoparticles used, we can predict the productivity of PSD under different operating conditions such as the climatic conditions of radiation intensity, air temperature and wind velocity. It is also possible to predict the temperature of both the distilled water and glass temperature under the same conditions.

As a result, when specifying a level for every factor, the model predicts its response. When the value of a group of variables in the equation is fixed, the previous equations show the expected change in the response of the only variable remaining in the equation. The mean of the total response for all solution runs can be obtained by intercepting the orthogonal design. By investigating the above equations, some very small coefficients can be noticed. Any small coefficient indicates that the associated term is not significant. For each mathematical model, the relation between the actual and predicted values were plotted as scatter diagrams as shown by Fig. 3a

Table 8
Residuals (R^2) for daily productivity (P) for different nanomaterials (Cu_2O, Al_2O_3, and TiO_2).

Nanomaterials (Cu_2O)						
Std. Dev.	Mean	C.V. %	R^2	Adjusted R^2	Predicted R^2	S/N ratio
82.3	5682.7	1.45	0.99	09808	0.9427	43.6
Nanomaterials (Al_2O_3)						
128.6	5239.	2.45	0.97	0.9441	0.8334	24.2
Nanomaterials (TiO_2)						
49.72	4637.5	1.07	0.99	0.9864	0.9899	43.9653

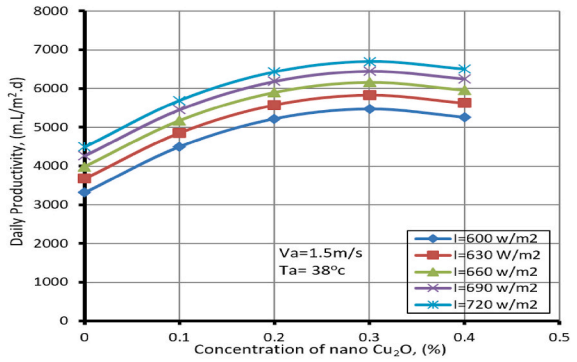

a. 2D curves

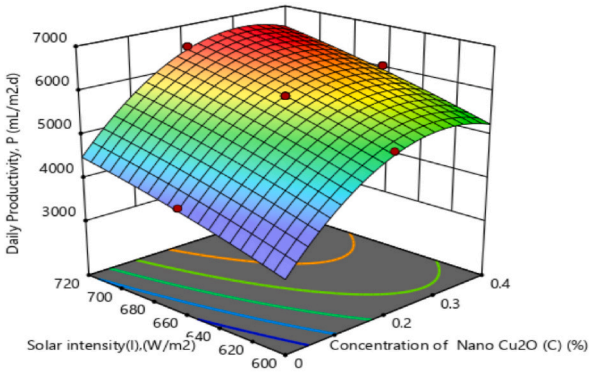

b. Surface plot (3D plot)

Fig. 4. Effect of concentration of nano Cu_2O on daily productivity at different levels of solar intensity (hold values: T_a = 38 °C and V_a = 1.5 m/s).

for the daily productivity responses. The scatter diagrams show the quality of the developed mathematical equations, where the predicted values are in sufficient agreement with the experimental.

Moreover, the ANOVA analysis was implemented for each mathematical relation. For the proposed equation of daily productivity (P), ANOVA results are obtained in Table 5, where it shows that the model F-value of 106.55 implies the model is significant. There is only a 0.01% chance that an F-value this large could occur due to noise. P-values less than 0.0500 indicate that model terms are significant. In this case, X_1, X_2, X_3, X_4, X_1X_4, X_2X_4, ${X_1}^2$ are significant model terms. Values greater than 0.1000 indicate that the model terms are not significant. If there are many insignificant model terms, model reduction may improve the model. For response 2 (water temperature, T_w), the model F-value of 411.01 implies that the model is significant. There is only a 0.01% chance that an F-value this large could occur due to noise. P -values less than 0.0500 indicate that the model terms are significant. In this case, X_2, X_3, X_1X_2, X_1X_3, X_1X_4, X_2X_3, X_2X_4, ${X_2}^2$ are significant model terms. Values greater than 0.1000 indicate that the model terms are not significant. If there are many insignificant model terms, model reduction may improve the model. For response 3 (glass temperature (T_g), the model is significant due to the F-value of 80.15. Here, the noise can affect F-value by only a 0.01% chance. The modelling terms would be significant if P -values are lower than 0.05. Then, X_1, X_2, X_3, X_4, X_1X_2, X_1X_3, X_1X_4, X_2X_3, X_2X_4, X_3X_4, ${X_1}^2$, ${X_2}^2$, ${X_4}^2$ are significant parameters. While, the model term would be insignificant, if the P -values are more than 0.1.

Where df, SS, and MS are the degree of freedom, sum of squares, and mean square, respectively.

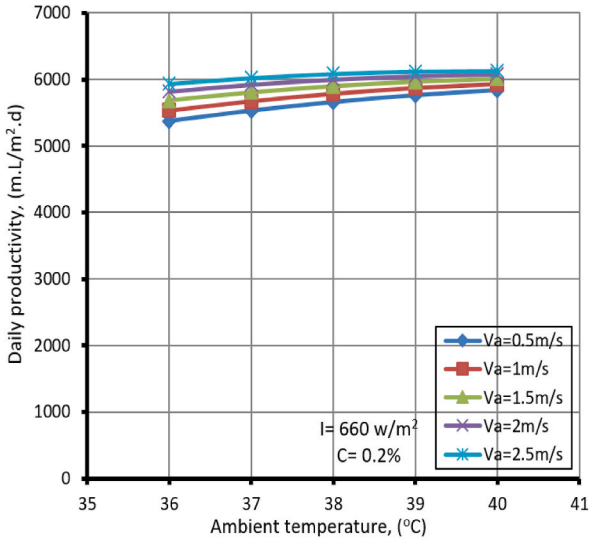

a. 2D curves

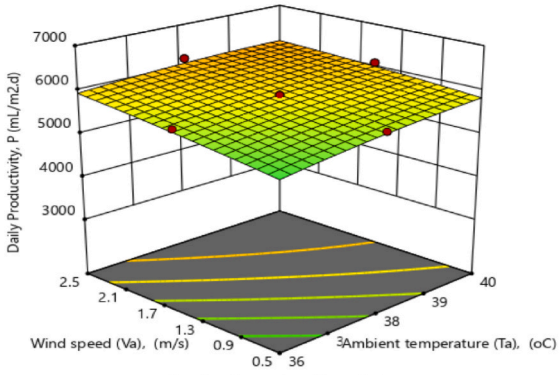

b. Surface plot (3D plot)

Fig. 5. Effect of ambient temperature on daily productivity of PSD at different levels of wind speed (hold values: (C) = 0.2% and (I) = 660 w/m^2).

4. Model validation

The experimental and model results are drawn for water daily productivity in Fig. 3a. The results obtained in Fig. 3a and ANOVA for P, T_w and T_g revealed that the frameworks (Equations (3)–(5)) are extremely significant and capable to symbolize the function between the inputs and responses with P $<$ 0.05 and high determination coefficient (R^2 =0.9900, 0.9974 and 0.9868 for P, T_w and T_g, respectively). Besides, the developed response models for P, T_w and T_g were examined using the residual analyses as illustrated in Fig. 3b for daily productivity. For normal residuals, the data are drawn in almost straight-line form. The existence of straight-line shape means that the values of experimentations and models for the responses are in a good relationship as revealed in Fig. 3a and b. It was emphasized that the tendency to have negative and positive values in residual analyses obtains the presence of some correlations [63]. Based on the above tables and figures and as a whole analyses of residuals for the responses, the built models do not show inadequacy. For daily productivity (P) of nanomaterials Cu_2O, the Predicted R^2 of 0.9427 is in reasonable agreement with the Adjusted R^2 of 0.9808; i.e., the difference is less than 0.4. Adeq Precision measures the signal to noise ratio as shown in Table 8. The consideration of the signal to noise ratio (S/N) is also important, S/N $>$ 4 is preferred. The S/N of 43.559 indicates an adequate signal. This model can be used to navigate the design space. The error existed among the experimental and coded values for P, T_w and T_g lies within 3.4%, 7.2%, and 4%, respectively. Moreover, the daily productivity (P) of nanomaterials Al_2O_3, the Predicted R^2 of 0.8334 is in reasonable agreement with the Adjusted R^2 of 0.9441; i.e., the difference is less than 0.12. Adeq Precision measures the signal to noise ratio as shown in Table 8. The consideration of the signal to noise ratio (S/N) is also important, S/N $>$ 4 is preferred. The S/N of 24.2 indicates an adequate signal. This model can be also used The error existed among the experimental and predicted value for P lies within 5.4%. Finally, the daily productivity (P) of nanomaterials TiO_2, the Predicted R^2 of 0.9899 is in reasonable agreement with the Adjusted R^2 of 0.9864; i.e., the difference is less than 0.1. Adeq Precision measures the signal to noise ratio as shown in Table 8. The consideration of the signal to noise ratio (S/N) is also important, S/N $>$ 4 is preferred. The S/N of 43.9653 indicates an adequate signal. The error existed among the experimental and coded values for P, T_w and T_g lies within 5.2%, 4.9%, and 6.5%, respectively. Evidently, this affirms the excellence of reproducibility of the pilot experimental results.

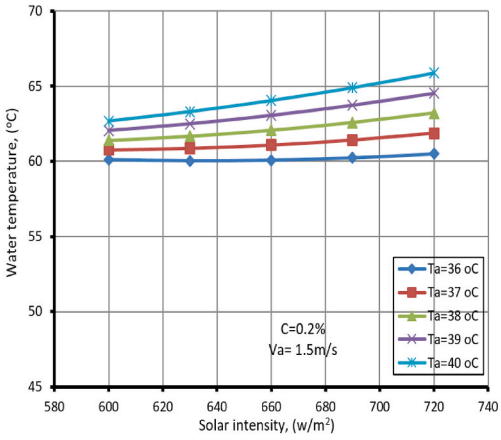

a. 2D curves.

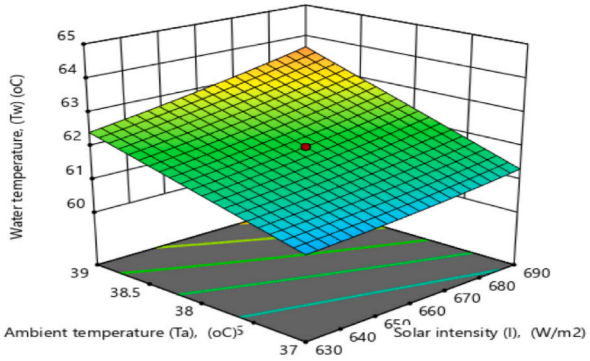

b. Surface plot (3D plot).

Fig. 6. Effect of solar intensity on water temperature (T_w) at different levels of ambient temperatures.

5. Results and discussion

The parametric analyses were conducted to obtain the impact of the input parameters like nanoparticles concentration (C), solar radiation (I), ambient temperature (T_a), and wind velocity (V_a) on the process responses of the productivity (P), water temperature (Tw), and glass temperature (Tg) during the day through RSM. Also, to examine the response variety, 3-D surface figures are created using RSM quadratic modeling. The relation between the inputs and responses of factors could be better understood using these charts.

5.1. Effect of input parameters on daily productivity of PSD

Fig. 4 illustrates the effect of concentration of Cu_2O nanoparticles on daily productivity of PSD at different levels of solar intensity (hold values: $T_a = 38$ °C and $V_a = 1.5$ m/s). The effect of solar intensity and concentration of nanoparticles on the daily productivity of PSD is also shown in Fig. 4b (Surface plot). The daily productivity varies non-linearly with solar intensity and concentration. It can be found that the productivity increases with raising the content of nanoparticles until it reaches a maximum value at the concentration of 0.3%, then the distillate decreases after that. The increase in productivity is thought due to the good effect of nanomaterials, which improves the thermal and heat transfer characteristics. While the productivity was reduced after the concentration of 0.3% due to the agglomeration of nanoparticles at the base because of the high content of nanomaterials in the base fluid. As a result, the fresh water productivity of PSD was increased from 5500 to 6800 mL/m^2.day when increasing the nanoparticles concentration from zero to 0.3%, respectively at the conditions of 720 W/m^2, 1.3 m/s, and 38 °C for the solar radiation, wind velocity, and ambient temperature, respectively. This means that the productivity was improved by 24% under these conditions.

Moreover, Fig. 4 shows that the solar still productivity is increased with increasing the solar radiation. This is in agreement with Rahbar and Esfahani [64], who stated that the solar radiation has a direct strong impact on the distiller performance. The solar intensity heats up the basin water and increases the convective heat transfer coefficient, which leads to evaporate the basin water quickly. Through the solar still device, the energy transfer processes consist of supplying the heat for basin water evaporation and removing it from generated vapor at the condensing surface (glass cover and condensers if applicable). As a result, under the operating conditions of 0.3%, 1.5 m/s, and 38 °C for the nanoparticles concentration, wind velocity, and ambient temperature, respectively, the distiller productivity was enlarged from 4500 mL/m^2.day to 6800 mL/m^2.day (improvement percentage = 51%) when increasing the

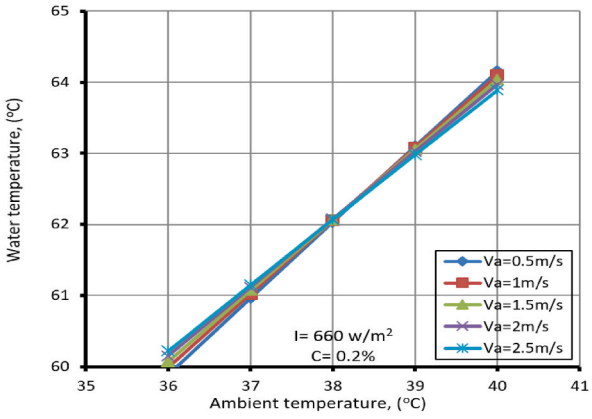

a. 2D curves.

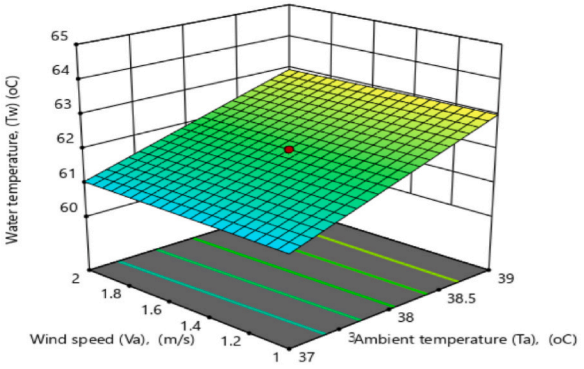

b. Surface plot (3D plot).

Fig. 7. Effect of ambient temperature on water temperature (T_w) at different levels of wind speeds (hold: (C) = 0.2% and (I) = 660 w/m^2).

solar radiation from 600 W/m^2 to 720 W/m^2, respectively.

Furthermore, the effect of the ambient temperature and wind speed on daily productivity of PSD in surface plot form is illustrated in Fig. 5. The daily productivity varies linearly with the ambient temperature and wind speed. It is observed from the figure that the productivity increases with the ambient temperature and wind speed, within the limits of measurements. The figure obtains that the temperature of surrounding air has a significant role on the solar distiller productivity. This is in agreement with Alheefi [65]. So, the PSD productivity was increased from 5400 to 5800 mL/m^2.day (improvement percentage = 7.4%) with increasing the ambient temperature from 36 °C to 40 °C when the nanoparticles concentration, solar radiation, and wind velocity were 0.2%, 660 W/m^2, and 0.5 m/s, respectively. Also, when the ambient temperature is increased, the rate of heat loss from the walls of the distiller decreases, so the temperature of the distilled water increases, and this leads to an increase in productivity. Besides, it was noted that this rate of increase in productivity decreases with increasing the air speed, so it was found that at a speed of 2.5 m/s and when the temperature rises from 36 to 40 °C, the productivity increases from 5900 to 6100 mL/m^2.day with an improvement percent of 3.4%. This may be due to the occurrence of some scattering of sunlight at high speeds.

Unlike the solar radiation and air temperature, the air speed has insignificant role of the output yield of the solar distillers. As the air velocity increases on the glass cover, it cools down and its temperature decreases. As well known, the solar still yield is improved by declining the glass cover temperatures. This is due to that decreasing the glass temperatures raises the difference between the vapor and glass temperatures, which leads to enhance the condensation process of the generated vapor on the glass inner surface. Hence, the productivity is improved, and this agrees with El-Sebaii [66]. As a result, at a nanoparticle concentration of 0.2%, a radiation intensity of 660 W/m^2, and an air temperature of 38 °C, the PSD productivity increases from 5750 to 6050 mL/m^2.day (improvement percent of 5%) when the air velocity increases from 0.5 to 2.5 m/s. Also, when the ambient temperature increases, the rate of heat loss decreases from the walls of the distiller, so the temperature of the distilled water increases, and this leads to an increase in productivity. It was noted Fig. 5 that the rate of increase in productivity decreases with the increase in air speed because increasing the air speed leads to scatter the sun's rays.

5.2. *Effect of input parameters on water temperatures of PSD*

Fig. 6 shows the effect of radiation intensity and air temperature on the temperature of distilled water (T_w) at a constant air speed of

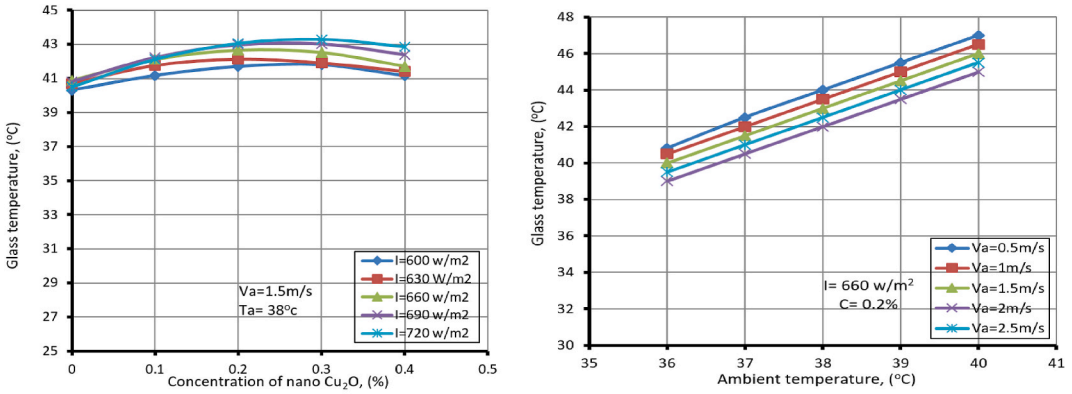

a. Effect of concentration of Cu_2O nanoparticles

b. Impact of ambient temperature

Fig. 8. Effect of concentration of Cu_2O nanoparticles and ambient temperature on the glass temperature (T_g).

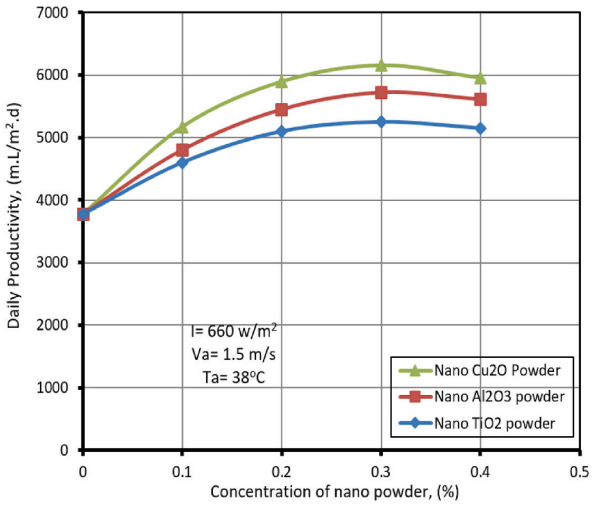

Fig. 9. The effect of nanoparticles concentration on the daily productivity considering different types of nanomaterials (hold values: I = 660 w/m^2, Va = 1.5 m/s, Ta = 38 °C).

1.5 m/s and nanoparticles concentration of 20%. It is obtained from Fig. 6 that the water temperature increases with increasing the radiation intensity at all temperature levels. Also, it was found that when the air temperature was 40 °C, the water temperature was 62.5 °C and 66 °C at the solar intensities of 600 and 720 W/m^2, respectively.

In addition, Fig. 6 shows an increase in T_w with increasing the air temperature (T_a) because the rate of heat losses decreases with raising the air temperature, and at the same time, the feed water temperature is almost equal to the air temperature. Then, as the air temperature increases, the temperature of the feed water increases, and therefore the temperature of the distilled water increases. As a result, at a solar radiation of 660 W/m^2, the temperature of distilled water increases from 60.5 to 63.5 °C when the air temperature changes from 36 to 40 °C.

Moreover, Fig. 7 demonstrates the effects of wind velocity and air temperature on the water temperature of PSD at a constant solar radiation of 660 W/m^2 and constant nanoparticles concentration of 20%. It is revealed from Fig. 7 that the effect of air velocity is marginal on T_w within the limits of the tested air velocities.

5.3. *Effect of input parameters on glass temperatures of PSD*

Fig. 8a illustrates the effect of the Cu_2O nanoparticles concentration and solar radiation on the glass temperature at constant air temperature and wind velocity. It is noted that the curve of the glass temperature with nanoparticles is similar to the curve of productivity with nanoparticles, where the glass temperature increases with raising the Cu_2O concentration to 0.3% and decreases after that. This is due to the increase in the rate of evaporation inside the distiller with increasing the water temperature at 0.3%, thus

increasing the condensation rate and raising the temperature of the glass. Also, Fig. 8a obtains that the temperature of the glass increases with increasing the solar radiation.

Fig. 8b shows the effect of the ambient temperature on the glass temperature (T_g) under different levels of wind speeds and constant nanoparticles concentration of 0.2% and solar radiation of 660 w/m^2. It can be concluded from Fig. 8b that both air velocity and air temperature have a significant effect on the glass temperature of the distiller. Besides, the air velocity is inversely proportional to the temperature of the glass because the glass will cool down when increasing the air velocity, and thus its temperature will decrease. While the air temperature is directly proportional to the glass temperature of the distiller, as increasing the air temperature increases the glass temperature.

5.4. Effect of using nanoparticles (TiO_2, Al_2O_3, and CuO) on the daily productivity of PSD

As well known, mixing the saline water with nanoparticles improves the absorptivity and thermal conductivity of the water basin. The impact of various nanomaterials mixed with the water basin on the PSD performance was studied. Three different nanomaterials were used (TiO_2, Al_2O_3 and Cu_2O). The selection of these nanomaterials was considered according to their optical, thermophysical, and heat transfer properties such as the thermal conductivity and specific heat capacity. For example, the thermal conductivities of CuO, Al_2O_3 and TiO_2 are 76.5, 40, and 11.8 W/m.K, respectively as presented in Table 1.

Fig. 9 shows the daily productivity of PSD when using different nanoparticles mixed with saline water. The results generally revealed that the best performance of PSD was obtained when using Cu_2O followed by Al_2O_3 and TiO_2, respectively as observed from Fig. 9. This is because the copper oxide and aluminum oxide nanoparticles helped to absorb more energy and reach to higher temperatures than that when using TiO_2 and conventional PSD. It was revealed that, in the case of Cu_2O nanoparticles, the average temperature difference between the water with nano of Cu_2O-PSD and the water of conventional PSD are 2.4 °C higher for Cu_2O-PSD. In addition, it was observed in the case of Al_2O_3 nanoparticles that the temperature of water with nano of Al_2O_3-PSD was higher than the water temperatures of PSD by 2.1 °C. Moreover, the temperature of the water when using TiO_2 was more than that of PSD by 1.9 °C. As a result of the high temperatures of PSD with nano-water, it gives the highest productivity when using Cu_2O followed by Al_2O_3 and then TiO_2 as shown in Fig. 9. The average daily productivity of the Cu_2O-PSD, Al_2O_3-PSD and TiO_2-PSD at nano-concentration of C = 0.3% was 6150, 5720 and 5300 mL/m^2.day compared to 3900 mL/m^2.day for that of the conventional PSD. So, the average daily productivity increase of Cu_2O-PSD, Al_2O_3-PSD and TiO_2-PSD was 57, 46 and 36% over the PSD, respectively.

5.5. The most important and most contributed parameters for each response

The percent of contribution for each source in the ANOVA tables for all responses is indicated in Tables 5–7. Table 5 indicated that the most influential and proportion in participation and importance is X_1 (concentration of nano) about 50% contribution, then X_2 (solar intensity) about 24.4% and then X_4 (Wind velocity) about 2.5%, on productivity (P). For T_w, Table 6 indicated that the most influential and proportion in participation and importance is X_3 (ambient temperature) about 65% and then X_2 (solar intensity) about 18%. For T_g, Table 7 indicated that the most contribution is X_4 (wind velocity) about 5% and then X_2 (solar intensity) about 4.8%.

5.6. Process multi-response optimization

A single optimal solution can be presented by single response optimization method. In principle, the proposed RSM gives not only one optimal solution but also sets of optimal solutions. In this investigation, three responses were employed, i.e. (P), (T_w), and (T_g). For the production goal, the preferred mixing of condition level must set the max (P), (T_w), and min (T_g). The selection of (P), (T_w) and (T_g) relies on the evaporation condition and user. Desirability is another name for RSM. It is a modern method for problems which is used to optimize multiple quality characteristic [67]. The desirability function, D (X) is a method which transforms an estimated response into a scale free value (di) called desirability and makes the use of an objective function. The range of D (X) was ranging from zero to one. Zero value argues that a response or more are outside the satisfactory boundaries, and one represents the ideal case. The individual desirability's weighted geometric mean for the responses was called as composite desirability. The optimal parameter conditions are considered to be the factor settings with maximum total desirability. The optimization is achieved by the simultaneous objective function, which is a geometric mean of all transformed responses.

Combined or composite desirability (CD) can be acquired by combining the individual desirability's [68] to find the best input parameters and increase the composite desirability. The individual desirability is evaluated if a response is to be maximized as:

$$d_i = \begin{cases} 0 & i < L_i \\ \dfrac{i - L_i}{T_i - L_i} \times r_i & L_i < i < T_i \\ 1 & i > T_i \end{cases} \quad (6)$$

The individual desirability is evaluated if a response is to be minimized as:

$$d_i = \begin{cases} 0 & i > H_i \\ \dfrac{H_i - i}{H_i - T_i} \times r_i & T_i < i < H_i \\ 1 & i < T_i \end{cases} \quad (7)$$

The individual desirability is evaluated if a response is targeted as:

Table 9
Input conditions and responses limitations of solar evaporation process.

Name	objective	Li	Hi	Lower W	Upper W	Importance
Concentration of Cu_2O, (C), (%)	Is in range	0	0.4	1	1	1
Solar intensity, (I), (w/m^2)	Is in range	600	720	1	1	1
Ambient temperature, (Ta), (^oC)	Is in range	36	40	1	1	1
Wind speed, (Va), (m/s)	Is in range	0.5	2.5	1	1	1
Productivity, ($m.L/m^2.d$)	Max	4050	6500	1	1	1
Water temperature, (Tw), (^oC)	Max	60	64.1	1	1	1
Glass temperature, (Tg), (^oC)	Min	38	46	1	1	1
Desirability, (D)	Max	0	0.956588	1	1	1

Table 10
High value of desirability for process conditions combinations.

Number	Process parameters				Predicted responses			Desirability, (D)
	(C), (%)	(I), (w/m^2)	(Ta), (^oC)	(Va), (m/s)	(P), ($m.L/m^2.d$)	(Tw), (^oC)	(Tg), (^oC)	
1	0.199	610.786	39.132	1.040	5252.06	62.19	43.83	0.79466
2	0.195	720	38.559	0.500	6469.96	64.10	38.09	0.41421
3	0.341	719.925	36.394	2.112	6461.47	62.22	42.81	0.99226
4	0.4	600.0	36.0	2.5	5343.33	62.10	23.17	0.59688
5	0.107	600.000	40.000	0.556	4222.45	63.67	41.65	0.64664
6	0.133	720.000	40.000	0.502	6089.97	66.66	31.12	0.32468
7	0.4	720.0	40.0	0.5	6840.0	64.4	42.8	0.94077
8	0.043	600.000	37.099	2.245	4252.03	60.25	41.10	0.73681
9	0.4	600	36.0	2.5	5343.33	62.10	23.17	0.14579
10	0.007	720.000	38.712	1.410	4627.36	64.10	38.00	0.64664
11	0.400	720.000	36.000	2.500	6140.00	62.87	39.43	0.61768
12	0.4	600.0	40.0	2.5	5556.67	62.47	42.83	0.78815
13	0.400	720.000	36.075	2.500	6144.70	62.93	39.59	0.52710
14	0.003	720.000	40.000	1.686	4649.42	66.02	38.00	0.78806
15	0.400	720.000	40.000	1.842	6424.08	65.51	45.31	0.62544
16	0.400	720.000	37.123	2.500	6194.92	63.77	41.76	0.43703
17	0.195	720.000	38.559	0.500	6469.96	64.10	38.09	0.75282

$$d_i = \begin{cases} \dfrac{i - L_i}{T_i - L_i} \times r_i & L_i < i < T_i \\ \dfrac{H_i - i}{H_i - T_i} \times r_i & T_i < i < H_i \\ 0 & H_i < i < L_i \end{cases} \tag{8}$$

where, i = the expected ith response, T_i = goal value for ith response, L_i = lesser suitable values for ith response, H_i = largest suitable values for ith response, $di = D(X)$ for ith response, CD = composite desirability, r_i = desirability function's weight of the ith response, w_i = the ith response's importance and $W = \Sigma w_i$.

If, the composite desirability is evaluated when the importance is the same for each response as:

$$\mathrm{CD} = (\mathrm{d_i} * \mathrm{d_2} * \ldots \mathrm{d_n})^{\frac{1}{n}} = \left[\prod(\mathrm{diwi})\right]^{\frac{1}{W}} \tag{9}$$

where n = responses' number. To reveal the differences in the responses' importance, where the weight wi fulfills $0 < w_i < 1$ and $w_1 + w_2 + w_3 + \ldots \ldots + w_n = 1$.

The main target of the optimization process is the identification of the input factors in the excremental range that maximizing P, T_w and minimizing T_g. This optimization process was conducted using MINITAB-15 software. The weight of each response is considered equal.

Table 9 presents the goal, responses, limitations of input conditions and weights assigned to each condition. The respects of 17 levels compoundings of operating factors that would furnish high values of composite desirability (0.99226–0.14579), and the values of expected responses acquired are yielded, Table 10.

Fig. 10 illustrates the optimized graphs of the three responses (P, T_w, and T_g) for nanomaterials Cu_2O, one response (P) for nanomaterials (Al_2O_3 and TiO_2), and optimization results for nanomaterials (Cu_2O, Al_2O_3 and TiO_2). The vertical lines symbolize the optimal circumstances, and horizontal dotted lines refer to the values of response. The composite desirability (D) was 0.99226, 1 and 1 for Cu_2O, Al_2O_3 and TiO_2, respectively. Table 11 obtains the optimal input parametric setting for RSM optimization. The optimal process parameter settings are concentration of Cu_2O, (C), 0.1948%, ambient temperature of 38.559 °C, wind speed of 0.5 m/s, and solar intensity of 720 w/m^2. Also, the optimal process parameter settings are concentration of Al_2O_3, (C), 0.40%, ambient temperature

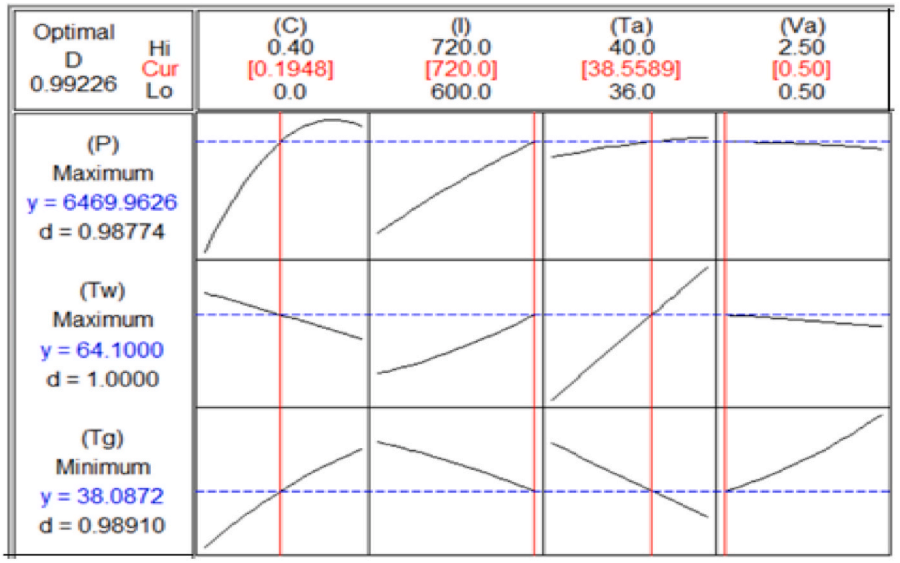

a. Multi-objective optimization results for (P), (T_w) and (T_g) of solar evaporation process for nanomaterial Cu_2O.

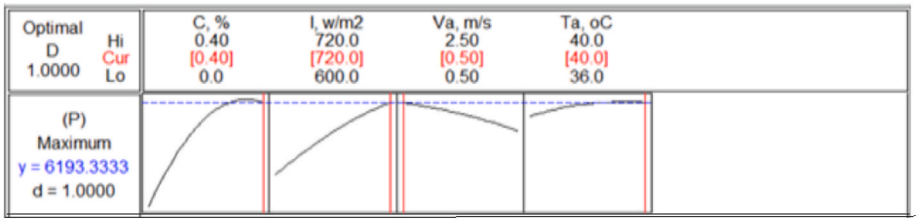

b. Multi-objective optimization results for (P), of solar evaporation process for nanomaterial Al_2O_3.

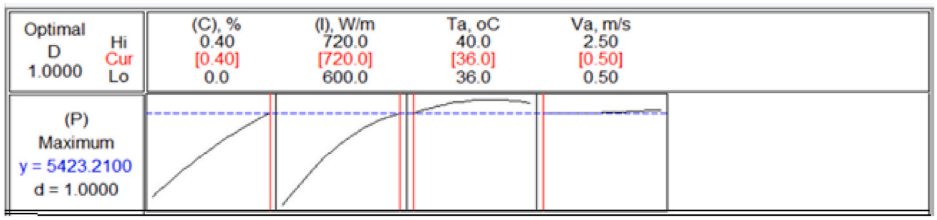

c. Multi-objective optimization results for (P), of solar evaporation process for nanomaterial TiO_2.

Fig. 10. Multi-objective optimization results of solar evaporation process for nanomaterials (Cu_2O, Al_2O_3 and TiO_2).

Table 11
Limitations of parameters and optimum parameters for nano powder Cu_2O solar evaporation process.

Parameter	Limitations of parameters	Optimum parameters
Concentration of Cu_2O, (C), (%)	0–0.4	0.1948
Solar intensity, (I), (w/m^2)	600–720	720
Ambient temperature, (Ta), (°C)	36–40	38.559
Wind speed, (Va), (m/s)	0.5–2.5	0.5

of 40 °C, wind speed of 0.5 m/s, and solar intensity of 720 w/m^2, and the optimal process parameter settings are concentration of TiO_2, (C), 0.40%, ambient temperature of 36 °C, wind speed of 0.5 m/s, and solar intensity of 720 w/m^2. In addition, Table 12 gives the expected optimum responses for Cu_2O solar evaporation process.

5.7. Comparability among this study and relevant investigations

The increase in productivity of the proposed PSD is compared with that of the previous investigations found in the literature to get

Table 12
Validation of models at optimum circumstances for Cu_2O, Al_2O_3 and TiO_2 nanomaterial in solar evaporation process.

Response	Type of nano materials	Objective	Expected optimum responses	Experimental	Error (%)
Productivity, (mL/m^2.d)	Cu_2O	Maximize	6469.96	6700	3.4
	Al_2O_3		6193.3	6550	5.4
	TiO_2		5423.2	5930	8.5
Water temperature, (T_w), (°C)	Cu_2O	Maximize	64	69	7.2
Glass temperature, (T_g), (°C)		Minimize	38.1	39.7	4

Table 13
Comparability among this study and relevant investigations.

Reference	PSD with modifications	Increase in productivity
Alawee et al. [49]	PSD with rotating cylinders and electric heaters	214%
Taamneh and Taamneh [69]	PSD with free and forced convection.	25%
Modi and Nayi [51]	PSD with forced evaporation, granite as a heat storing material, and forced condensation	61.53%
Kabeel et al. [70]	PSD with corrugated plate and PCM.	87.4%
Kabeel and Abdelgaied [54]	PSD with graphite absorber and cooling of glass.	107.7%
Alawee et al. [52]	PSD with dangled wick ropes	122%
Manokar et al. [71]	PSD with insulation conditions and 1 cm water depth.	19.46%
Saravanan and Murugan [72]	PSD with wick and 2 cm water depth.	40.3%
Essa et al. [50]	PSD with mirrors, cooling cycle, and wick dangled cords	195%
Present study	PSD with nanomaterials (Cu_2O, Al_2O_3 and TiO_2).	57%

how much the improvement be achieved with the performance of PSD with nanomaterials. This comparability is presented in Table 13. The comparability obtained the effectiveness of the introduced modifications conducted on PSD.

6. Conclusions

The present work introduces a mathematical modeling using a novel technique for predicting the freshwater productivity and temperatures of water and glass of PSD. The regression models for predicting the performance parameter responses were developed using RSM and a four-factor, five-level central composite architecture. Based on the above explanation, the following points can be withdrawn.

1. RSM evidenced that it is an efficient tool for analyzing the performance of PSD with Cu_2O, Al_2O_3 and TiO_2 nanoparticles.
2. The comprehensive introduced models built utilizing RSM have quite unique, powerful, and flexible methodology for PSD of Cu_2O, Al_2O_3 and TiO_2 nanoparticles.
3. An optimization study has also been submitted to get maximum P or maximum T_w and minimum T_g under the different working conditions for PSD with Cu_2O, Al_2O_3 and TiO_2 nanoparticles respectively.
4. The observed optimal process parameter settings based on composite desirability were concentrations of Cu_2O nanoparticles of 19.5%, solar intensity of 720 w/m^2, ambient temperature of 38.6 °C, and wind speed of 0.5 m/s for achieving the maximum P of PSD or maximum T_w and minimum T_g. Also, the optimal process parameter settings of (Al_2O_3-PSD) and (TiO_2-PSD) process are their concentrations of 40%, wind speed of 0.5 m/s, solar intensity of 720 w/m^2 and ambient temperature of 40 °C, for (Al_2O_3-PSD) process, and 36 °C for (TiO_2-PSD) process, respectively.
5. The anticipated values well match the experimental data (R^2 of 0.99, 0.9974 and 0.9868 for P, T_w and T_g, for (Cu_2O-PSD) process respectively. Moreover R^2 of 0.97 and 0.99 for P of (Al_2O_3-PSD) process and (TiO_2-PSD) process respectively.
6. Cu_2O-PSD process has proved its suitability with acceptable P that reached 6469.96 mL/m^2.day, T_w which reached 64 °C, and T_g less than 38.1 °C. Moreover, when using (Al_2O_3-PSD) process and (TiO_2-PSD) process, their acceptable values for P reached to 6193.3 mL/m^2.day and 5423.21 mL/m^2.day, respectively.
7. The best performance of PSD was obtained when using (Cu_2O-PSD) process followed by (Al_2O_3-PSD) process and (TiO_2-PSD) process, respectively. Also, the highest productivity was obtained at the nanoparticle's concentrations of 0.3% under all environmental conditions, where the PSD productivity recorded 6800 mL/m^2.day at the conditions of 720 W/m^2, 1.3 m/s, and 38 °C for the solar radiation, wind velocity, and ambient temperature, respectively.
8. The water temperature of PSD depends mainly on the solar radiation and ambient temperature. The more the solar radiation and ambient temperature, the more the water temperature. On contrast, the effect of air velocity is marginal on the distiller water temperature within the limits of the tested air velocities.
9. The glass temperature of PSD relies mainly on the ambient temperature and concentration of nanomaterials used. The glass temperature was highest at the nanoparticle's concentration achieved the highest productivity. Also, the more the ambient temperature, the more the glass temperature. Besides, increasing the wind velocity reduces the glass temperature.
10. A good matching between the results of the proposed RSM model and actual experimental data was obtained. The error for water productivity, water temperature, and glass temperature of (Cu_2O-PSD) lies within 3.4%, 7.2%, and 4%, respectively. In

addition, the error between the experimental and predicted values for water productivity, lies within 5.4% and 8.5%, for (Al_2O_3-PSD) and (TiO_2-PSD) respectively.

Authors' contributions to the published work

W.M. Farouk: Manufacture of the experimental setup, conducting practical experiments, **A.S. Abdullah:** Design experimental setup and participate in analyzing the results., **Suha A. Mohammed:** Manufacture of the experimental setup, conducting practical experiments, **Wissam H. Alawee:** Participate in developing the idea of research and developing it, Participating in analyzing the results and writing the manuscript., **Z.M. Omara:** Participate in developing the idea of research, participation in analyzing the results and reviewing the manuscript., **F.A. Essa:** Participate in developing the idea of research and developing it,

Declaration of competing interest

The authors declare that they have no known competing financial interests or personal relationships that could have appeared to influence the work reported in this paper.

Acknowledgment

The authors extend their appreciation to the Deputyship for Research & Innovation, Ministry of Education in Saudi Arabia for funding this research work through the project number (IF-PSAU-2021/01/17978).

References

[1] H. Lv, Y. Wang, L. Wu, Y. Hu, Numerical simulation and optimization of the flash chamber for multi-stage flash seawater desalination, Desalination 465 (2019) 69–78.
[2] A.S. Abdullah, Z.M. Omara, M. Bek, F.A. Essa, An augmented productivity of solar distillers integrated to HDH unit: experimental implementation, Appl. Therm. Eng. 167 (2020) 114723.
[3] F.A. Essa, A.S. Abdullah, Z.M. Omara, A.E. Kabeel, W.M. El-Maghlany, On the different packing materials of humidification–dehumidification thermal desalination techniques – a review, J. Clean. Prod. (2020) 123468.
[4] C. Ghenai, D. Kabakebji, I. Douba, A. Yassin, Performance analysis and optimization of hybrid multi-effect distillation adsorption desalination system powered with solar thermal energy for high salinity sea water, Energy 215 (2021) 119212.
[5] F.A. Essa, A.H. Elsheikh, R. Sathyamurthy, A.M. Manokar, A.E. Kandeal, S. Shanmugan, A. Kabeel, S.W. Sharshir, H. Panchal, M. Younes, Extracting water content from the ambient air in a double-slope half-cylindrical basin solar still using silica gel under Egyptian conditions, Sustain. Energy Technol. Assessments 39 (2020) 100712.
[6] S. Thampy, G.R. Desale, V.K. Shahi, B.S. Makwana, P.K. Ghosh, Development of hybrid electrodialysis-reverse osmosis domestic desalination unit for high recovery of product water, Desalination 282 (2011) 104–108.
[7] M.A. Jamil, S.M. Elmutasim, S.M. Zubair, Exergo-economic analysis of a hybrid humidification dehumidification reverse osmosis (HDH-RO) system operating under different retrofits, Energy Convers. Manag. 158 (2018) 286–297.
[8] A.S. Abdullah, F.A. Essa, Z.M. Omara, Effect of different wick materials on solar still performance–a review, Int. J. Ambient Energy (2019) 1–28.
[9] Z.M. Omara, A.E. Kabeel, M.M. Younes, Enhancing the stepped solar still performance using internal reflectors, Desalination 314 (2013) 67–72.
[10] A.S. Abdullah, A. Alarjani, M.M.A. Al-sood, Z.M. Omara, A.E. Kabeel, F.A. Essa, Rotating-wick solar still with mended evaporation technics: experimental approach, Alex. Eng. J. 58 (4) (2019) 1449–1459.
[11] Z.M. Omara, A.S. Abdullah, A.E. Kabeel, F.A. Essa, The cooling techniques of the solar stills' glass covers–a review, Renew. Sustain. Energy Rev. 78 (2017) 176–193.
[12] S.W. Sharshir, G. Peng, L. Wu, F.A. Essa, A.E. Kabeel, N. Yang, The effects of flake graphite nanoparticles, phase change material, and film cooling on the solar still performance, Appl. Energy 191 (2017) 358–366.
[13] F.A. Essa, Z.M. Omara, A.S. Abdullah, S. Shanmugan, H. Panchal, A.E. Kabeel, R. Sathyamurthy, Wissam H. Alawee, A.M. Manokar, A.H. Elsheikh, Wall-suspended trays inside stepped distiller with Al_2O_3/paraffin wax mixture and vapor suction: experimental implementation, Energy Storage 32 (2020) 102008.
[14] F.A. Essa, Z.M. Omara, A.S. Abdullah, S. Shanmugan, H. Panchal, A.E. Kabeel, R. Sathyamurthy, M.M. Athikesavan, A. Elsheikh, M. Abdelgaied, B. Saleh, Augmenting the Productivity of Stepped Distiller by Corrugated and Curved Liners, CuO/paraffin Wax, Wick, and Vapor Suctioning, Environmental Science and Pollution Research, 2021.
[15] F.A. Essa, A.S. Abdullah, Z.M. Omara, Rotating discs solar still: new mechanism of desalination, J. Clean. Prod. 275 (2020) 123200.
[16] M.M. Younes, A.S. Abdullah, Z.M. Omara, F.A. Essa, Enhancement of discs' solar still performance using thermal energy storage unit and reflectors: an experimental approach, Alex. Eng. J. 61 (10) (2022) 7477–7487.
[17] F.A. Essa, F.S. Abou-Taleb, M.R. Diab, Experimental Investigation of Vertical Solar Still with Rotating Discs, Energy Sources, Part A: Recovery, Utilization, and Environmental Effects, 2021, pp. 1–21.
[18] M.R. Diab, F.A. Essa, F.S. Abou-Taleb, Z.M. Omara, Solar Still with Rotating Parts: a Review, Environmental Science and Pollution Research, 2021.
[19] A.S. Abdullah, F.A. Essa, Z.M. Omara, Y. Rashid, L. Hadj-Taieb, G.B. Abdelaziz, A.E. Kabeel, Rotating-drum solar still with enhanced evaporation and condensation techniques: comprehensive study, Energy Convers. Manag. 199 (2019) 112024.
[20] A.S. Abdullah, Z.M. Omara, A. Alarjani, F.A. Essa, Experimental investigation of a new design of drum solar still with reflectors under different conditions, Case Stud. Therm. Eng. 24 (2021) 100850.
[21] F.A. Essa, A.S. Abdullah, Z.M. Omara, Improving the performance of tubular solar still using rotating drum–Experimental and theoretical investigation, Process Saf. Environ. Protect. 148 (2021) 579–589.
[22] M. Abdelgaied, Y. Zakaria, A.E. Kabeel, F.A. Essa, Improving the tubular solar still performance using square and circular hollow fins with phase change materials, J. Energy Storage 38 (2021) 102564.
[23] A. Kabeel, R. Sathyamurthy, A.M. Manokar, S.W. Sharshir, F. Essa, A.H. Elshiekh, Experimental study on tubular solar still using Graphene Oxide Nano particles in Phase Change Material (NPCM's) for fresh water production, J. Energy Storage 28 (2020) 101204.
[24] F.A. Essa, A.S. Abdullah, Wissam H. Alawee, A. Alarjani, Umar F. Alqsair, S. Shanmugan, Z.M. Omara, M.M. Younes, Experimental enhancement of tubular solar still performance using rotating cylinder, nanoparticles' coating, parabolic solar concentrator, and phase change material, Case Stud. Therm. Eng. 29 (2022) 101705.
[25] A.S. Abdullah, M. Younes, Z.M. Omara, F.A. Essa, New design of trays solar still with enhanced evaporation methods–Comprehensive study, Sol. Energy 203 (2020) 164–174.
[26] A.S. Abdullah, Z.M. Omara, F.A. Essa, M.M. Younes, S. Shanmugan, M. Abdelgaied, M.I. Amro, A.E. Kabeel, W.M. Farouk, Improving the performance of trays solar still using wick corrugated absorber, nano-enhanced phase change material and photovoltaics-powered heaters, Energy Storage 40 (2021) 102782.

[27] F.A. Essa, A.S. Abdullah, Z.M. Omara, A.E. Kabeel, Y. Gamiel, Experimental study on the performance of trays solar still with cracks and reflectors, Appl. Therm. Eng. 188 (2021) 116652.
[28] F.A. Essa, Z.M. Omara, A.S. Abdullah, A.E. Kabeel, G.B. Abdelaziz, Enhancing the solar still performance via rotating wick belt and quantum dots nanofluid, Case Stud. Therm. Eng. (2021) 101222.
[29] Z. Haddad, A. Chaker, A. Rahmani, Improving the basin type solar still performances using a vertical rotating wick, Desalination 418 (2017) 71–78.
[30] Z.M. Omara, A.S. Abdullah, F.A. Essa, M.M. Younes, Performance evaluation of a vertical rotating wick solar still, Process Saf. Environ. Protect. 148 (2021) 796–804.
[31] A. Kabeel, Z.M. Omara, F. Essa, A. Abdullah, T. Arunkumar, R. Sathyamurthy, Augmentation of a solar still distillate yield via absorber plate coated with black nanoparticles, Alex. Eng. J. 56 (2017) 433–438.
[32] A.E. Kabeel, Z.M. Omara, F.A. Essa, Numerical investigation of modified solar still using nanofluids and external condenser, J. Taiwan Inst. Chem. Eng. 75 (2017) 77–86.
[33] H. Panchal, H. Nurdiyanto, K.K. Sadasivuni, S.S. Hishan, F.A. Essa, M. Khalid, S. Dharaskar, S. Shanmugan, Experimental investigation on the yield of solar still using manganese oxide nanoparticles coated absorber, Case Stud. Therm. Eng. 25 (2021) 100905.
[34] S. Shanmugan, F.A. Essa, S. Gorjian, A.E. Kabeel, R. Sathyamurthy, A. Muthu Manokar, Experimental study on single slope single basin solar still using TiO2 nano layer for natural clean water invention, J. Energy Storage 30 (2020) 101522.
[35] F.A. Essa, Wissam H. Alawee, Suha A. Mohammed, H.A. Dhahad, A.S. Abdullah, Z.M. Omara, Experimental investigation of convex tubular solar still performance using wick and nanocomposites, Case Stud. Therm. Eng. 27 (2021) 101368.
[36] A.S. Abdullah, Z.M. Omara, Habib Ben Bacha, M.M. Younes, Employing convex shape absorber for enhancing the performance of solar still desalination system, J. Energy Storage (2021) 103573.
[37] Wissam H. Alawee, Suha A. Mohammed, Hayder A. Dhahad, F.A. Essa, Z.M. Omara, A.S. Abdullah, Performance analysis of a double-slope solar still with elevated basin- comprehensive study, Desalination Water Treat. 223 (2021) 13–25.
[38] M.E.H. Attia, A.E. Kabeel, M. Abdelgaied, F.A. Essa, Z.M. Omara, Enhancement of hemispherical solar still productivity using iron, zinc and copper trays, Sol. Energy 216 (2021) 295–302.
[39] A.M. Manokar, Y. Taamneh, A. Kabeel, R. Sathyamurthy, D.P. Winston, A.J. Chamkha, Review of different methods employed in pyramidal solar still desalination to augment the yield of freshwater, Desalination Water Treat. 136 (2018) 20–30.
[40] K.H. Nayi, K.V. Modi, Pyramid solar still: a comprehensive review, Renew. Sustain. Energy Rev. 81 (2018) 136–148.
[41] W.M. Alaian, E.A. Elnegiry, A.M. Hamed, Experimental investigation on the performance of solar still augmented with pin-finned wick, Desalination 379 (2016) 10–15.
[42] A.M. Manokar, D.P. Winston, Experimental analysis of single basin single slope finned acrylic solar still, Mater. Today Proc. 4 (2017) 7234–7239.
[43] Z.M. Omara, M.H. Hamed, A.E. Kabeel, Performance of finned and corrugated absorbers solar stills under Egyptian conditions, Desalination 277 (2011) 281–287.
[44] Z.M. Omara, A.E. Kabeel, F.A. Essa, Effect of using nanofluids and providing vacuum on the yield of corrugated wick solar still, Energy Convers. Manag. 103 (2015) 965–972.
[45] M.M. Younes, A.S. Abdullah, F.A. Essa, Z.M. Omara, M.A. Amro, Enhancing the wick solar still performance using half barrel and corrugated absorbers, Process Saf. Environ. Protect. 150 (2021) 440–452.
[46] A.E. Kabeel, Z.M. Omara, F.A. Essa, Improving the performance of solar still by using nanofluids and providing vacuum, Energy Convers. Manag. 86 (2014) 268–274.
[47] A.S. Abdullah, F.A. Essa, H.B. Bacha, Z.M. Omara, Improving the trays solar still performance using reflectors and phase change material with nanoparticles, J. Energy Storage 31 (2020) 101744.
[48] A.E. Kabeel, Z.M. Omara, F.A. Essa, A.S. Abdullah, Solar still with condenser–A detailed review, Renew. Sustain. Energy Rev. 59 (2016) 839–857.
[49] A.E. Kabeel, Z.M. Omara, F.A. Essa, Enhancement of modified solar still integrated with external condenser using nanofluids: an experimental approach, Energy Convers. Manag. 78 (2014) 493–498.
[50] H. Al-Madhhachi, G.F. Smaisim, Experimental and numerical investigations with environmental impacts of affordable square pyramid solar still, Sol. Energy 216 (2021) 303–314.
[51] A. Prakash, R. Jayaprakash, Performance evaluation of stepped multiple basin pyramid solar still, Mater. Today Proc. 45 (2021) 1950–1956.
[52] Wissam H. Alawee, Suha A. Mohammed, H.A. Dhahad, A.S. Abdullah, Z.M. Omara, F. Essa, Improving the performance of pyramid solar still using rotating four cylinders and three electric heaters, Process Saf. Environ. Protect. 148 (2021) 950–958.
[53] F.A. Essa, Wissam H. Alawee, Suha A. Mohammed, A.S. Abdullah, Z.M. Omara, Enhancement of pyramid solar distiller performance using reflectors, cooling cycle, and dangled cords of wicks, Desalination 506 (2021) 115019.
[54] K.V. Modi, K.H. Nayi, Efficacy of forced condensation and forced evaporation with thermal energy storage material on square pyramid solar still, Renew. Energy 153 (2020) 1307–1319.
[55] Wissam H. Alawee, F.A. Essa, Suha A. Mohammed, H.A. Dhahad, A.S. Abdullah, Z.M. Omara, Y. Gamiel, Improving the performance of pyramid solar distiller using dangled cords of various wick materials: novel working mechanism of wick, Case Stud. Therm. Eng. 28 (2021) 101550.
[56] M. Elgendi, M.Y.E. Selim, A. Aldhaheri, W. Alshehhi, H. Almarshoodi, A. Alhefeiti, Design procedures for a passive pyramid solar still with an automatic feed water system, Alex. Eng. J. 61 (2022) 6419–6431.
[57] A.E. Kabeel, M. Abdelgaied, Enhancement of pyramid-shaped solar stills performance using a high thermal conductivity absorber plate and cooling the glass cover, Renew. Energy 146 (2020) 769–775.
[58] V. Shanmugapriya, K. Mohanapandian, P. Periasamy, K. Senthilkannan, K. Amudha, B. Selvakumar, Enhanced properties of Zn2+ substituted Cr2O3 nanoparticles in escalating the distillate yield of acrylic pyramid solar still, Mater. Today Proc. 49 (2022) 1579–1589.
[59] Z. Kim, Y. Shin, J. Yu, G. Kim, S. Hwang, Development of NOx removal process for LNG evaporation system: comparative assessment between response surface methodology (RSM) and artificial neural network (ANN), J. Ind. Eng. Chem. 74 (2019) 136–147.
[60] F. Paulo, L. Santos, Double emulsion solvent evaporation approach as a novel eugenol delivery system–Optimization by response surface methodology, Ind. Crop. Prod. 126 (2018) 287–301.
[61] T.A. El-Taweel, S. Gouda, Performance analysis of wire electrochemical turning process—RSM approach, Int. J. Adv. Manuf. Technol. 53 (2011) 181–190.
[62] D.C. Montgomery, Design and Analysis of Experiments, John wiley & sons, 2017.
[63] A.I. Khuri, S. Mukhopadhyay, Response surface methodology, Wiley Interdiscip. Rev.: Comput. Stat. 2 (2010) 128–149.
[64] N. Rahbar, J.A. Esfahani, Experimental study of a novel portable solar still by utilizing the heatpipe and thermoelectric module, Desalination 284 (2012) 55–61.
[65] T. Alheefi, Experimental and Analytical Study of Water Production of Solar Still, Brunel University London, 2019.
[66] A. El-Sebaii, On effect of wind speed on passive solar still performance based on inner/outer surface temperatures of the glass cover, Energy 36 (2011) 4943–4949.
[67] G. Derringer, R. Suich, Simultaneous optimization of several response variables, J. Qual. Technol. 12 (1980) 214–219.
[68] T. El-Taweel, Multi-response optimization of EDM with Al–Cu–Si–TiC P/M composite electrode, Int. J. Adv. Manuf. Technol. 44 (2009) 100–113.
[69] Y. Taamneh, M.M. Taamneh, Performance of pyramid-shaped solar still: experimental study, Desalination 291 (2012) 65–68.
[70] A.E. Kabeel, M.A. Teamah, M. Abdelgaied, G.B. Abdel Aziz, Modified pyramid solar still with v-corrugated absorber plate and PCM as a thermal storage medium, J. Clean. Prod. 161 (2017) 881–887.
[71] A. Muthu Manokar, Y. Taamneh, A.E. Kabeel, D. Prince Winston, P. Vijayabalan, D. Balaji, R. Sathyamurthy, S. Padmanaba Sundar, D. Mageshbabu, Effect of water depth and insulation on the productivity of an acrylic pyramid solar still – an experimental study, Groundwater Sustain. Dev. 10 (2020) 100319.
[72] A. Saravanan, M. Murugan, Performance evaluation of square pyramid solar still with various vertical wick materials – an experimental approach, Therm. Sci. Eng. Prog. 19 (2020) 100581.